ACS Photonics

Article

pubs.acs.org/journal/apchd5

Surface Enhanced Raman Spectroscopy Using a Single Mode Nanophotonic-Plasmonic Platform

Frédéric Peyskens,*[,†] Ashim Dhakal,[†] Pol Van Dorpe,[‡,§] Nicolas Le Thomas,[†] and Roel Baets[†]

[†]Photonics Research Group, INTEC, Ghent University-imec, Center for Nano- and BioPhotonics, Ghent University, Sint-Pietersnieuwstraat 41, 9000 Ghent, Belgium

[‡]imec, Kapeldreef 75, 3001 Heverlee, Belgium

[§]Department of Physics, KULeuven, Celestijnenlaan 200D, 3001 Leuven, Belgium

Supporting Information

ABSTRACT: We demonstrate the generation of Surface Enhanced Raman Spectroscopy (SERS) signals from integrated bowtie antennas, excited and collected by the fundamental TE mode of a single mode silicon nitride waveguide. Due to the integrated nature of this particular single mode SERS probe one can rigorously quantify the complete enhancement process. The Stokes power, generated by a 4-nitrothiophenol-coated antenna and collected into the fundamental TE mode, exhibits an 8×10^6 enhancement compared to the free space Raman scattering of a 4-nitrothiophenol molecule. Furthermore, we present an analytical model which identifies the relevant design parameters and figure of merit for this new SERS-platform. An excellent correspondence is obtained between the theoretically predicted and experimentally observed absolute Raman power. This work paves the way toward a new class of fully integrated lab-on-a-chip systems where the single mode SERS probe can be combined with other photonic, fluidic, or biological functionalities.

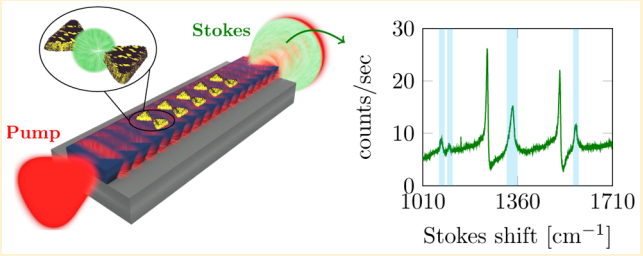

KEYWORDS: *surface enhanced raman spectroscopy, single mode waveguide, photonic integrated circuits, bowtie nanoantenna, plasmonic modeling*

Surface Enhanced Raman Spectroscopy (SERS) is a promising technique for enhancing inherently weak Raman signals by introducing a plasmonic nanostructure in the vicinity of the analyte under study.[1−12] SERS spectra have mainly been generated using simple plasmonic substrates or colloidal solutions of metallic nanoparticles, whereby the signal is excited and collected by a conventional microscopy system. Recently, photonic integrated circuits (PICs) emerged as a promising alternative to standard confocal microscopy to probe spontaneous Raman spectra.[13] The fundamental building block of such circuits is a single mode waveguide in which the pump and Stokes light is guided in a high-index core material surrounded by lower-index cladding materials. While researchers also started integrating nanoplasmonic antennas on top of such waveguides,[14−20] PICs have only been used to probe SERS signals from external, nonintegrated, metallic nanoparticles.[21−23] Such an approach is, however, poor in terms of quantitative results owing to the large uncertainty on the Raman enhancement and coupling between the excitation beam and the metallic nanoparticles.[24] In order to obtain quantitative SERS spectra a complete control of the plasmonic enhancement and coupling with the underlying waveguide is necessary.

Here we present a new class of SERS probes that overcomes these issues. We demonstrate for the first time the generation of SERS signals from integrated bowtie nanoantennas, excited and collected by a single mode silicon nitride waveguide. Due to the fully integrated nature of the developed single mode SERS probe it is possible to rigorously quantify the complete enhancement and coupling process. We show that the SERS spectra can be attributed to a genuine plasmon resonance effect and experimentally determine the enhanced Stokes power, generated by a single nanoantenna, which is coupled into the fundamental TE mode. Furthermore, an analytical model identifying the relevant design parameters and figure of merit for waveguide-based SERS is developed as well. The theoretically predicted absolute Raman power perfectly corresponds with the experimentally observed power coupled into the fundamental TE mode. Finally, we discuss the impact of the shot noise resulting from the inherent silicon nitride Raman background and outline the interplay between signal optimization and noise reduction in order to achieve the optimal absolute detection limit.

A schematic of the device under study is shown in Figure 1a. The fundamental TE mode of a silicon nitride (SiN) rib waveguide excites a periodic array of $\mathcal{N}$ gold bowtie antennas coated with a 4-nitrothiophenol (NTP) monolayer. The pump wavelength for all experiments is set to λ_p = 785 nm and NTP

Received: September 3, 2015
Published: December 9, 2015

DOI: 10.1021/acsphotonics.5b00487
ACS Photonics 2016, 3, 102−108

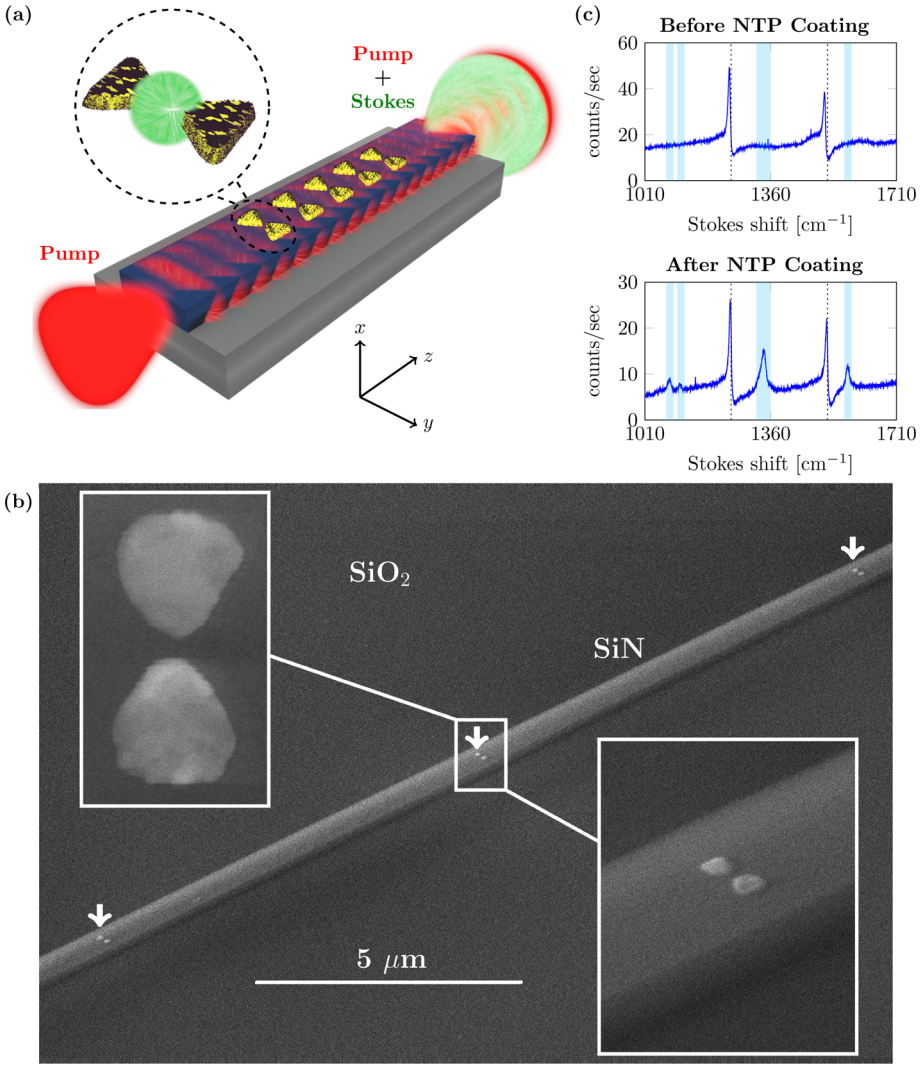

Figure 1. Evanescent excitation and collection of SERS spectra. (a) Schematic of the chip consisting of single mode SiN waveguides (blue) on an SiO_2 undercladding (gray), functionalized with an array of gold bowtie antennas (yellow). All antennas are coated with an NTP monolayer (purple dots), evanescently excited by the fundamental TE mode (red). The NTP Stokes signal (green) is collected by the same mode. (b) Scanning electron microscope image of a functionalized waveguide. The white arrows indicate antenna positions. The insets show a zoom of a typical antenna. (c) Raman spectra of a waveguide functionalized with 40 antennas. The cyan shaded areas mark the NTP Stokes peaks while the black dashed lines represent peaks attributed to interference effects of the plasmonic array. Before coating, the waveguide already generates a Raman background in itself (top). After coating, NTP peaks emerge (bottom).

Stokes light (at λ_S) is subsequently collected back into the same waveguide mode. Fabrication details can be found in the Methods section and a description of the measurement setup is outlined in the Supporting Information, S1. A scanning electron microscope image of the functionalized waveguide, i.e. a waveguide patterned with plasmonic nanoantennas, is depicted in Figure 1b. All waveguides have a cross-sectional area of 220 × 700 nm^2. Raman spectra of an uncoated (without NTP) and coated (with NTP) waveguide functionalized with 40 antennas are shown in Figure 1c. The spectral regions where an NTP Stokes peak is expected (1080, 1110, 1340, and 1575 cm^{-1})[25] are highlighted by the cyan shaded areas. Before coating, no NTP peaks can be distinguished from the inherent SiN background. After coating, four additional peaks appear and coincide with the expected NTP Stokes peaks. This demonstrates that SERS signals from single monolayer coated antennas can indeed be excited and collected by the same fundamental waveguide mode. The peaks at 1250 and 1518 cm^{-1} (marked by the black dashed lines) are attributed to interference effects of the Au array which act on the scattered background light, and they are also observed on the extinction curves of the functionalized waveguides (see Supporting Information, S2). Hence, they do not represent specific Raman lines.

Subsequently, the dependence of the SERS signal on the position of the plasmon resonance was investigated to verify that it can be attributed to a resonance effect and not to coincidental surface roughness. To this end, waveguides functionalized with a fixed number of antennas (N = 20) but varying bowtie geometries were considered. The relevant bowtie parameters are its length L, gap Δ, and apex angle α (Figure 2a) and by changing the length one can tune the antenna resonance (extinction). The single antenna extinction spectra $E(\lambda)$ (in dB) are calculated through $E(\lambda) = (T_{ref}(\lambda) - T_{Nant}(\lambda))/N$ in which $T_{ref}(\lambda)$ is the power transmission through a reference waveguide and $T_{Nant}(\lambda)$ is the power transmission

DOI: 10.1021/acsphotonics.5b00487
ACS Photonics 2016, 3, 102−108

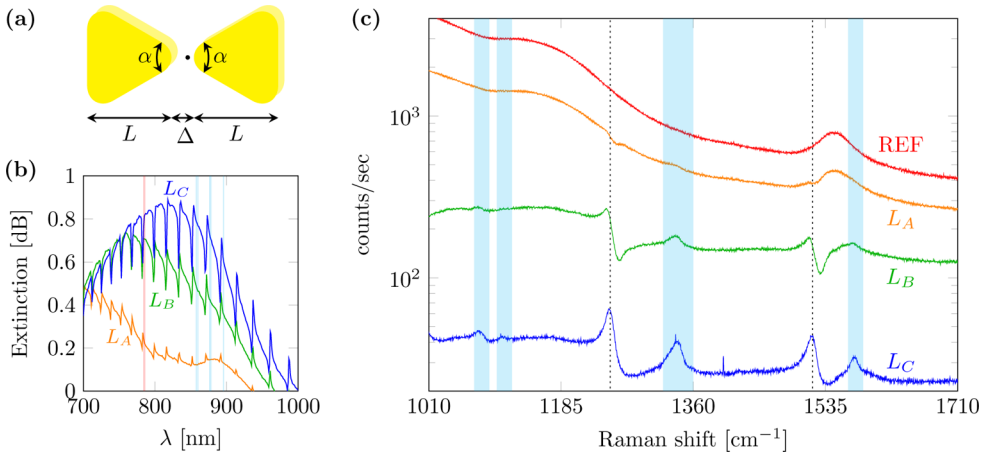

Figure 2. Signal dependence on the plasmon resonance. (a) Geometrical parameters of a bowtie antenna: length L, gap Δ, and apex angle α. (b) Single antenna extinction spectra for three different $\alpha \approx 60°$ bowtie antennas with fixed gap $\Delta \approx 51 \pm 13$ nm but varying length: $L_A \approx 95 \pm 8$ nm (orange), $L_B \approx 110 \pm 12$ nm (green), and $L_C \approx 125 \pm 13$ nm (blue). The red and cyan shaded lines correspond to the pump and Stokes wavelengths, respectively. (c) Corresponding Raman spectra of the waveguides functionalized with these three bowtie anntenas (orange, green, and blue) and Raman spectrum of the reference waveguide (red).

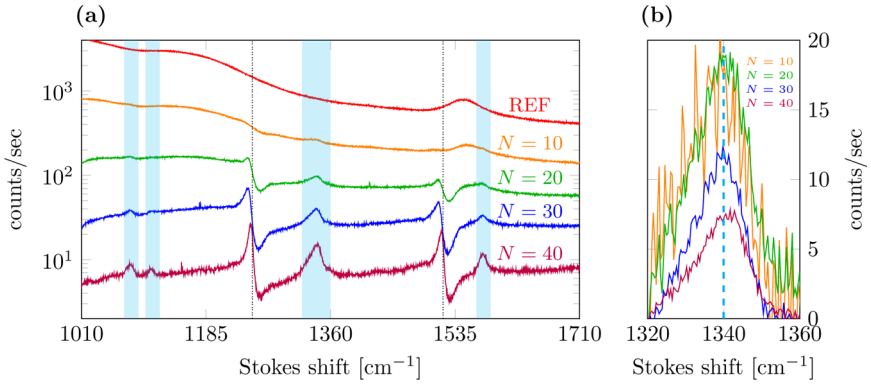

Figure 3. Signal dependence on the number of antennas N. (a) Raman spectra of a reference waveguide (REF) and waveguides functionalized with N = 10, 20, 30, and 40 antennas. (b) Zoom on the 1340 cm^{-1} signal peak. The background is locally subtracted to obtain the pure NTP signal.

of a waveguide functionalized with N antennas (see Supporting Information, S2, for more details).[14] Figure 2b depicts such single antenna extinction spectra for three different $\alpha \approx 60°$ bowties ($L_A \approx 95 \pm 8$ nm, $L_B \approx 110 \pm 12$ nm, and $L_C \approx 125 \pm 13$ nm with fixed $\Delta \approx 51 \pm 13$ nm), while the corresponding Raman spectra are shown in Figure 2c. The Raman spectrum of a reference waveguide without any Au functionalization is also shown. Even after coating the reference waveguide does not generate NTP peaks, so any Raman signal indeed originates from the antenna region and does not contain contributions from spontaneous Raman scattering along the waveguide.[13] The L_A resonance is detuned from the relevant pump and Stokes region, resulting in a poor Raman spectrum. By increasing the length (L_B and L_C bowties), the resonance redshifts and lines up with the pump and Stokes wavelengths. For these bowties the NTP spectrum starts to emerge. The reported SERS spectra can hence be attributed to a plasmon resonance effect such that a stable and reproducible enhancement factor can be associated with them, in contrast to SERS events originating from random surface defects. The increased overlap with the plasmon resonance, and hence extinction, also results in a decreased background.

Due to the metal induced loss, there will exist an optimum number N_{opt} of patterned antennas such that the SERS signal is maximized. Such an optimum is investigated in Figure 3 for a fixed $\alpha \approx 60°$ bowtie geometry ($L \approx 106 \pm 8$ nm and $\Delta \approx 48 \pm 13$ nm) but varying N: N = 10, 20, 30, 40, and 70 and N = 0, which is a reference waveguide. Each waveguide is measured 10 times, and the averaged Raman spectra are reported in Figure 3a. The N = 70 signal is not shown since it could not be distinguished from the inherent offset signal of the detector. The reference waveguide generates a considerable background signal, resulting in background associated shot noise which will mask the smaller peaks. Functionalizing the waveguide with increasing N reduces this unwanted background due to the attenuation caused by the nanoantennas. In addition the dominant 1340 cm^{-1} peak starts to emerge when N increases. The smaller peaks at 1080, 1110, and 1575 cm^{-1} only appear when the background is sufficiently low. A zoom on the 1340 cm^{-1} peak (cyan dashed line) is shown in Figure 3b. For clarity, the background is locally subtracted. The signal reaches a maximum value for $10 \leq N \leq 20$ and then decays again with increasing N. The waveguides functionalized with N = 10 or 20 antennas hence show a better performance in terms of absolute signal enhancement compared to the N = 40 waveguide. In contrast, the reduced background in the N = 40 case allows to resolve the complete spectrum. In that respect the N = 40 waveguide exhibits a better performance, albeit at a reduced limit of detection since the signal enhancement is decreased. Apart from signal optimization, it is hence equally important to

DOI: 10.1021/acsphotonics.5b00487
ACS Photonics 2016, 3, 102−108

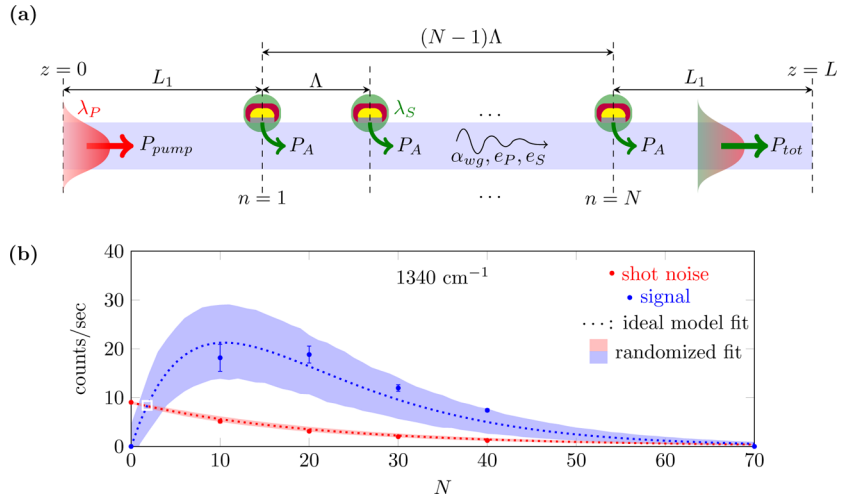

Figure 4. On-chip SERS model and fit to the experimental data. (a) Longitudinal cross-section of the chip. The pump beam, with power P_{pump} at wavelength λ_P, excites a Stokes signal λ_S of which the total power at the output facet is P_{tot}. The plasmonic array consists of N antennas with period Λ and is separated L_1 from both the input and output facet of the chip. Each of the antennas generates P_A guided Stokes power for a given pump power. Apart from the waveguide losses α_{wg}, the pump and Stokes light is attenuated by the pump e_P and Stokes e_S extinction, respectively. (b) Signal (blue circles) and shot noise (red circles) at the 1340 cm^{-1} peak. The dotted lines represent a constrained fit to the ideal model while the shaded areas represent a randomized fit to estimate the uncertainty on the experimental parameters. The white square denotes the minimum number of antennas N_{min} required to generate a detectable signal.

reduce the SiN background such that the smallest spectral features can be distinguished. In order to outline the interplay between signal enhancement and background reduction, we have developed an analytical model that incorporates all relevant design parameters and elucidates on the absolute detection performance.

Figure 4a shows a schematic longitudinal cross-section of the chip consisting of N antennas spaced with period $\Lambda = 10$ μm. Each array is centered on the waveguide with a distance $L_1 \approx 0.5$ cm to the front and back facet of the chip. The NTP monolayer on each antenna will generate a forward propagating Stokes power $P_A(\lambda_P, \lambda_S) = \eta_A(\lambda_P, \lambda_S)P_{pump}$ for a given pump power P_{pump}. The single antenna conversion efficiency $\eta_A(\lambda_P, \lambda_S)$ is an antenna-dependent factor incorporating the integrated field enhancement profile near the metal surface and the molecular density and Raman cross-section. The total transmission loss induced by one antenna at wavelength λ is given by $1 - e_\lambda^{-1}$, whereby e_λ is the linear antenna extinction. Apart from the intrinsic waveguide losses α_{wg}, the pump and Stokes light will hence also be attenuated by e_P and e_S, respectively. In the Supporting Information, S3, it is then shown that the total Stokes power P_{tot} generated by an array of N coated antennas is approximately given by

$$\frac{P_{tot}}{P_{pump}} \approx \eta_A(\lambda_P, \lambda_S) e^{-2\alpha_{wg}L_1} e_S^{(1-N)} \left(\frac{1 - \left(\frac{e_S}{e_P}\right)^N}{1 - \left(\frac{e_S}{e_P}\right)} \right)$$

$$= \mathrm{FOM}(N, \lambda_P, \lambda_S) e^{-2\alpha_{wg}L_1}$$

The quantity $\mathrm{FOM}(N, \lambda_P, \lambda_S)$ contains all necessary parameters to assess the SERS signal strength for a given waveguide geometry and is hence considered to be the relevant figure of merit (FOM) in comparing the performance of integrated antenna arrays. The optimum antenna number $N_{opt} = \log\{\log(e_S)/\log(e_P)\}/\log(e_S/e_P)$. For the particular bowtie antenna studied in Figure 3, the extinction spectrum $e(\lambda)$ and single antenna conversion efficiency $\eta_A(\lambda_P, \lambda_S)$ are numerically evaluated using Lumerical FDTD Solutions (see Methods). The predicted N_{opt} for the 1340 cm^{-1} peak is 8–9 antennas, using the simulated extinctions $e_P = 1.16$ ($E_P = 0.63$ dB) and $e_S = 1.10$ ($E_S = 0.43$ dB), while $\eta_A \approx 2.19 \times 10^{-15}$. For each 1 W of pump power, the antenna is therefore expected to generate 2.19 fW of guided Stokes power. The Raman enhancement factor is calculated through $EF_R = EF(\lambda_P)^2 EF(\lambda_S)^2$ in which $EF(\lambda)$ is the local field enhancement (see Methods). In the center of the gap at 5 nm from the tip of the antenna (marked by the black dot in Figure 2a), an $EF_R \approx 1.14 \times 10^4$ is expected. Due to the large gap the enhancement is relatively low. However, fabrication induced variations on a larger gap will have less pronounced effects on EF_R as compared to variations on a very narrow gap. Since our primary goal is to investigate the properties of this platform and establish whether our analytical model can faithfully reproduce the experimental data, it is more convenient to work with a larger gap and avoid possible large variations in EF_R. This allows a more reliable comparison between theory and experiment. Furthermore, it is interesting to assess the efficiency with which the total emitted Stokes radiation is coupled to the fundamental TE mode. The β-factor is a measure for this efficiency and is determined by the ratio of the Stokes power coupled into the fundamental TE mode P_{TE} and the total radiated Stokes power P_{rad}, $\beta = P_{TE}/P_{rad}$ (more details on the calculation of β can be found in the Methods). For the 1340 cm^{-1} line, $\beta \approx 17\%$ for a dipole in the center of the gap and at 15 nm above the top surface of the waveguide. The total modal power is equally distributed in forward and backward propagating TE light. As far as the pump efficiency is concerned, it is important to note that the pump power which is not used by the first antenna, is still fully available for the next antennas in the array (apart from a small waveguide loss reduction). In that respect it is possible to transfer almost all the pump light to the antennas, which makes the overall energy transfer quite efficient. It should be noted, however, that part of the exchanged power is lost due to nonradiative heating and, hence, does not contribute to the optical excitation. By sweeping the geometrical parameters, one

DOI: 10.1021/acsphotonics.5b00487
ACS Photonics 2016, 3, 102–108

could in principle find a configuration that optimizes the β-factor or the useful energy transfer. However, since the overall Raman process is a combination of two wavelength contributions, it is likely that a separate optimization of the structure for either the pump or Stokes light will not yield the optimal SERS signal; hence, it remains essential to optimize the suggested figure of merit as this eventually determines the maximal SERS signal. Apart from the relevant NTP signal, the SiN itself generates a considerable background while the pump beam is propagating along the waveguide. This background signal P_{bg} can be approximated by

$$\frac{P_{bg}}{P_{pump}} \approx \eta_B(\lambda_P, \lambda_S) e^{-2\alpha_{wg}L_1}(e_P^{-N} + e_S^{-N})L_1$$

in which $\eta_B(\lambda_P, \lambda_S)$ is a waveguide-dependent factor incorporating the specific modal field profile and the SiN molecular density and cross-section (see Supporting Information, S4). It is clear that the background increases linearly with the total propagation length ($\propto L_1$) and decays exponentially with the number of antennas. In order to achieve the highest signal-to-noise ratio (SNR) it is hence important to keep L_1 as short as possible.

Our analytical model and the associated numerical calculations will now be benchmarked against the spectra from Figure 3 to verify whether the theoretically estimated power values correspond to the experimentally obtained absolute Raman powers. To this end, the NTP signal strength at 1340 cm^{-1}, obtained from Figure 3b, is analyzed as a function of the antenna number N and compared with the theoretical estimations. Furthermore, the background associated shot noise is also calculated. The results are depicted in Figure 4b. While the ideal model assumes N identical antennas, the fabricated antennas will show differences among each other resulting in changes of e_P, e_S, and η_A from one antenna to the other. In order to incorporate potential differences of these parameters we have developed a generalized on-chip SERS model as described in the Supporting Information, S5. By applying a randomized fit to this generalized model, it is possible to estimate the uncertainty on the experimental parameters e_P, e_S, and η_A. For each of these three parameters, we generated a set of normally distributed numbers and plugged them into the generalized model to calculate the distribution of signal and shot noise counts. The obtained signal and shot noise distributions then define an area within which the probable signal (blue area) and noise (red area) counts are situated. The mean values of the original e_P, e_S, and η_A distributions are extracted from an initial constrained fit to the ideal model (dotted lines), while their standard deviations are chosen such that the eventual signal and shot noise distributions cover all experimental data points (red and blue dots). Based on the randomized fit, it is possible to estimate the spread on the experimental parameters: $E_P \approx 0.49 \pm 0.15$ dB, $E_S \approx 0.35 \pm 0.11$ dB, and $\eta_A = (2.60 \pm 0.77) \times 10^{-15}$ (theoretically, $E_P = 0.63$ dB, $E_S = 0.43$ dB, and $\eta_A = 2.19 \times 10^{-15}$ were predicted). The theoretically predicted parameters are all within the error bars of the experimentally fitted data, which clearly establishes the validity of our model and its ability to provide quantitative predictions of the absolute Raman power coupled into a single mode waveguide. Given this excellent correspondence, we expect the fabricated structures to have a Raman enhancement factor EF_R on the order of 1.14×10^4 near the two antenna gap tips. Decreasing the gap size should boost EF_R and η_A by another 2 or 3 orders of magnitude. From the fitted conversion efficiency η_A, one immediately derives that a single antenna produces (2.60 ± 0.77) fW of guided Stokes power for each 1 W of guided pump power. Compared to the free space Raman scattering P_0 of a single NTP molecule in a bulk air environment $P_A \approx 3.94 \times 10^6 P_0$. This includes the excitation and emission enhancement of all molecules in the monolayer, as well as the coupling efficiency to the guided mode. Since only half of the Stokes light is carried by the forward propagating mode, the total power coupled into the fundamental TE mode is therefore $\approx 8 \times 10^6 P_0$.

Our observations also reveal that a minimum number of antennas N_{min} is required to generate a detectable signal (marked by the white square in Figure 4b). If $N < N_{min}$, then the shot noise still dominates on the signal. It has to be noted, however, that the relevant signal is generated in a very small region $(N-1)\,\Lambda$ compared to the overall length $2L_1 + (N-1)\,\Lambda \approx 2L_1$, while the shot noise is mainly attributed to this nonuseful length $2L_1 \approx 10000$ μm. Practically the antenna section can be made as short as ≈ 10 μm for a single antenna. Consequently, designs in which dedicated on-chip splitters are used to separate the pump and Stokes light should in principle allow to reduce the background by a factor of 1000. These devices are therefore expected to have a $\sqrt{1000} \approx 32$ times higher SNR, pushing toward the $N_{min} = 1$ limit, such that signals generated by a single antenna can still be detected. As a result it would become possible to simultaneously probe large areas of analytes ($>\lambda^2$) and detecting all SERS events originating from different locations by monitoring just a single waveguide output, in contrast to microscopy based systems where one has to serially scan all hotspot locations. Background reduction through such designs is moreover important to relax the trade-off between signal enhancement and resolving the spectrum. As we have previously discussed, the smallest features of the NTP spectrum only become visible when the background is sufficiently low. For example, the 1110 cm^{-1} peak is visible for the L_C structures in Figure 2c, but not for the L_B ones. Despite this advantage of the L_C structures, the absolute SERS enhancement (and hence output signal strength) of the Stokes peaks itself is lower for the L_C structures as compared to the SERS enhancement of the L_B structures. Numerical simulations show that the figure of merit $FOM(N_{opt}, \lambda_P, \lambda_S)$ of each of the Stokes lines (always evaluated at the corresponding optimum antenna number N_{opt}) of the L_B structures is on average 1.51× higher than the corresponding $FOM(N_{opt}, \lambda_P, \lambda_S)$ of the L_C structures. This means that if one wants to resolve the total spectrum by reducing the background through antenna attenuation (so, e.g., replacing the L_B by L_C antennas), one might have to select a nanoplasmonic antenna array with a nonoptimal performance in terms of absolute SERS enhancement. The reason for this decrease of the figure of merit is that one either has to select a nonoptimal antenna number (for a given bowtie geometry) or select a nonoptimal bowtie geometry (for a fixed N) to allow a sufficient reduction of the background. In the example of Figure 2c, a nonoptimal bowtie geometry (L_C over L_B, for a fixed N) had to be selected to generate a substantial extinction of the background. Figure 3 exemplifies the other case in which a nonoptimal antenna number ($N = 40$) allows to completely resolve the spectrum, while the overall SERS signal strength is reduced as compared to the $N = 10$ or $N = 20$ case. When the background is reduced by a dedicated chip design, one maintains the possibility of

DOI: 10.1021/acsphotonics.5b00487
ACS Photonics 2016, 3, 102−108

optimizing the antenna array in terms of absolute SERS enhancement. Since N_{opt} is completely determined by λ_P and λ_S, the highest absolute SERS signal strength will then be obtained for an array geometry for which FOM($N_{opt}(\lambda_P, \lambda_S)$, λ_P, λ_S) ≡ FOM(λ_P, λ_S) is optimized for a given λ_P and λ_S. By numerical simulation one can show that for a fixed angle $\alpha \approx 60°$ and gap $\Delta \approx 51$ nm, the optimal length $L \approx 110$ nm (for the given pump and Stokes wavelengths). The same procedure can be repeated for other gap sizes or other geometries. Hence, using our model it is possible to find an antenna array which maximizes the absolute on-chip SERS enhancement for a given pump and Stokes wavelength.

In conclusion, we have fabricated a fully integrated single mode SERS probe enabling on-chip excitation and emission enhancement in the 700−1000 nm region and developed an analytical model to outline the relevant design parameters and figure of merit for this new platform. It is shown that the SERS spectra can be attributed to a plasmon resonance effect and that the Stokes power coupled into the fundamental TE mode perfectly matches with the theoretical predictions extracted from our analytical model. As a result, the suggested platform enables a complete quantitative control on the Raman enhancement and subsequent coupling of the enhanced Stokes light with the underlying waveguide. Furthermore, we established, theoretically and experimentally, the existence of an optimal number of antennas to maximize the SERS signal and discussed the impact of the SiN background noise on the absolute detection limit, while providing strategies to simultaneously optimize the signal and mitigate the noise. The 700−1000 nm wavelength region is of particular interest for Raman sensing due to the low fluorescence, negligible water absorption and availability of high quality and low-cost sources and detectors.[26] In combination with other on-chip spectral functionalities, such as arrayed waveguide gratings,[26] the presented SERS probe is forecasted to allow multiplexed detection of extremely weak Raman signals on a highly dense integrated platform. We also envisage that integrated nano-antennas, similar to the ones reported here, could be used as transducer between quantum dot emitters and the fundamental waveguide mode, potentially enabling applications in on-chip quantum communication and quantum computation.[27,28]

METHODS

Fabrication Details. The fabrication consists of a two-step e-beam lithography process. In the first step, the nanoplasmonic antennas are patterned on top of a slab $Si/SiO_2/SiN$ wafer using a positive PMMA e-beam resist. After PMMA exposure, the samples are developed in a 1:1 MIBK:IPA solution after which a 2 nm Ti adhesion layer and 30 nm Au layer are deposited in a commercial Pfeiffer Spider sputter system. The samples are then immersed in acetone for lift-off. In the second step, the waveguides are defined. After metal lift-off, a negative ma-N 2403 resist is spun, exposed, and developed in ma-D 525. An e-spacer is also spun on top of the ma-N 2403 to avoid charging effects. The developed samples are then etched with an ICP plasma (C_4F_8/SF_6 mixture) in a commercial Oxford Plasmalab system. After resist strip and cleaning, the samples are immersed overnight in a 1 mM NTP:EtOH solution and subsequently rinsed with pure ethanol to remove the residual NTP. A self-assembled monolayer of NTP is assumed to form on the Au surface through a Au−S bond.[25]

Numerical Simulations. Numerical simulations were performed with Lumerical FDTD Solutions. We used a refractive index of $n_{rib} = 1.9$ for the SiN rib (with width $w_{rib} = 700$ nm and height $h_{rib} = 220$ nm), $n_{uclad} = 1.45$ for the SiO_2 undercladding and $n_{tclad} = 1$ for the top cladding (air). The Si substrate was not taken into account since the real oxide cladding is thick enough to avoid substantial power leakage to the Si such that the numerical results faithfully represent the actual experimental conditions. A thin native oxide layer ($t_{nox} = 2$ nm) between the SiN and the Ti has also been incorporated.[17] The metal stack thicknesses are fixed to $t_{Ti} = 2$ nm and $t_{Au} = 30$ nm and a built-in refractive index model for Au (Johnson and Christy[29]) and Ti (CRC[30]) is used. An additional surface layer with thickness $t_{NTP} = 1$ nm and index $n_{NTP} = 3$ is used to model the NTP monolayer. The antenna region (including the Ti adhesion layer and the NTP monolayer) is meshed with a uniform mesh of 0.5 nm in the plane of the antenna (yz-plane) and 2 nm in the x-direction. A mesh refinement to 1 nm (0.5 nm) is applied in regions where the thickness in the x-direction is ≤2 nm (≤1 nm). The estimated surface area of an NTP molecule is 0.18 nm^2, so the surface density is then $\rho_s = 5.56 \times 10^{18}$ molecules/m^2.[25] The Raman cross-section is $\sigma \approx 0.358 \times 10^{-30}$ cm^2/sr, which was obtained by applying the λ_S^{-4} scaling to the original data of the 1340 cm^{-1} line.[31] Single antenna extinction spectra $E(\lambda)$ (in dB) are calculated through $E(\lambda) = T_{ref}(\lambda) - T_{ant}(\lambda)$ in which $T_{ref}(\lambda)$ is the power transmission (in dB) through the reference waveguide and $T_{ant}(\lambda)$ is the power transmission (in dB) of a waveguide functionalized with one antenna. Linear extinction spectra $e(\lambda) \triangleq e_\lambda$ are then given by $e(\lambda) = 10^{E(\lambda)/10}$. A field and index profile monitor are used to extract the local field $|\mathbf{E}(\mathbf{r},\lambda)|$ and index $n(\mathbf{r})$ around the antenna. The single antenna conversion efficiency

$$\eta_A(\lambda_P, \lambda_S) = \frac{\rho_s \sigma}{2t_{NTP}} \frac{\iiint_{V_m} n_g(\lambda_P) n_g(\lambda_S) \lambda_S^2 |\mathbf{E}(\mathbf{r}, \lambda_P)|^2 |\mathbf{E}(\mathbf{r}, \lambda_S)|^2 d\mathbf{r}}{(\iint n(\mathbf{r})^2 |\mathbf{E}^m(\mathbf{r}, \lambda_P)|^2 d\mathbf{r})(\iint n(\mathbf{r})^2 |\mathbf{E}^m(\mathbf{r}, \lambda_S)|^2 d\mathbf{r})}$$

is calculated by integrating the local fields over the effective monolayer volume V_m in which the index satisfies $n(\mathbf{r})|_{\mathbf{r}\in V_m} = n_{NTP}$ (see Supporting Information, S3). The group index of the waveguide mode is $n_g(\lambda)$. The denominator is calculated using the modal fields $\mathbf{E}^m(\mathbf{r},\lambda)$ of a nonfunctionalized reference waveguide and the local field enhancement is given by the ratio of the local and modal electric fields: $EF(\mathbf{r}, \lambda) = \frac{|\mathbf{E}(\mathbf{r},\lambda)|}{|\mathbf{E}^m(\mathbf{r},\lambda)|}$. At a certain position, the Raman enhancement factor EF_R is calculated as $EF_R = EF(\lambda_P)^2 EF(\lambda_S)^2$. In order to determine the β-factor of the system we calculated the total radiated power P_{rad} and the power coupled to the fundamental TE mode P_{TE}. The β-factor is then given by $\beta = P_{TE}/P_{rad}$. For these calculations we considered a fixed dipole emitter source near the antenna surface. P_{rad} can then be calculated using a 3D power monitor of which the boundaries are in the far field of the dipole source. P_{TE} can be simultaneously determined using a mode expansion monitor that extracts the power carried by the TE mode. Numerically calculated values are mentioned in the main text.

ASSOCIATED CONTENT

Supporting Information

The Supporting Information is available free of charge on the ACS Publications website at DOI: 10.1021/acsphotonics.5b00487.

DOI: 10.1021/acsphotonics.5b00487
ACS Photonics 2016, 3, 102−108

A discussion of the SERS and plasmon resonance measurement setup, a derivation of the analytical on-chip SERS model and SiN background signal and a description of the randomized fit procedure applied to a generalized on-chip SERS model (PDF).

AUTHOR INFORMATION

Corresponding Author

*E-mail: fpeysken@intec.ugent.be.

Notes

The authors declare no competing financial interest.

ACKNOWLEDGMENTS

The authors acknowledge Josine Loo (imec) for performing the e-beam lithography, Liesbet Van Landschoot for making the SEM images, Ananth Subramanian for useful discussions, and Stephane Clemmen for providing feedback on the manuscript. This research was funded by the ERC Grant InSpectra. F.P. acknowledges support from the Bijzonder Onderzoeksfonds (BOF) fellowship of Ghent University.

REFERENCES

(1) Anker, J. N.; Hall, W. P.; Lyandres, O.; Shah, N. C.; Zhao, J.; Van Duyne, R. P. Biosensing with plasmonic nanosensors. *Nat. Mater.* **2008**, *7*, 442−453.

(2) Willets, K. A.; Van Duyne, R. P. Localized surface plasmon resonance spectroscopy and sensing. *Annu. Rev. Phys. Chem.* **2007**, *58*, 267−297.

(3) Halas, N. J.; Lal, S.; Chang, W.-S.; Link, S.; Nordlander, P. Plasmons in strongly coupled metallic nanostructures. *Chem. Rev.* **2011**, *111*, 3913−3961.

(4) Giannini, V.; Fernández-Domínguez, A. I.; Heck, S. C.; Maier, S. A. Plasmonic nanoantennas: fundamentals and their use in controlling the radiative properties of nanoemitters. *Chem. Rev.* **2011**, *111*, 3888−3912.

(5) Chu, Y.; Banaee, M. G.; Crozier, K. B. Double-resonance plasmon substrates for surface-enhanced Raman scattering with enhancement at excitation and Stokes frequencies. *ACS Nano* **2010**, *4*, 2804−2810.

(6) McFarland, A. D.; Young, M. A.; Dieringer, J. A.; Van Duyne, R. P. Wavelength-scanned surface-enhanced Raman excitation spectroscopy. *J. Phys. Chem. B* **2005**, *109*, 11279−11285.

(7) Ye, J.; Wen, F.; Sobhani, H.; Britt Lassiter, J.; Van Dorpe, P.; Nordlander, P.; Halas, N. J. Plasmonic Nanoclusters: Near Field Properties of the Fano Resonance Interrogated with SERS. *Nano Lett.* **2012**, *12*, 1660−1667.

(8) Kasera, S.; Biedermann, F.; Baumberg, J. J.; Scherman, O. A.; Mahajan, S. Quantitative SERS Using the Sequestration of Small Molecules Inside Precise Plasmonic Nanoconstructs. *Nano Lett.* **2012**, *12*, 5924−5928.

(9) Gallinet, B.; Siegfried, T.; Sigg, H.; Nordlander, P.; Martin, O. J. F. Plasmonic Radiance: Probing Structure at the Angström Scale with Visible Light. *Nano Lett.* **2013**, *13*, 497−503.

(10) Siegfried, T.; Ekinci, Y.; Martin, O. J. F.; Sigg, H. Gap Plasmons and Near-Field Enhancement in Closely Packed Sub-10 nm Gap Resonators. *Nano Lett.* **2013**, *13*, 5449−5453.

(11) Li, J.; Chen, C.; Jans, H.; Xiumei, X.; Verellen, N.; Vos, I.; Okumura, Y.; Moshchalkov, V. V.; Lagae, L.; Van Dorpe, P. 300 mm Wafer-level, ultra-dense arrays of Au-capped nanopillars with sub-10 nm gaps as reliable SERS substrates. *Nanoscale* **2014**, *6*, 12391−12396.

(12) Seok, T. J.; Jamshidi, A.; Eggleston, M.; Wu, M. C. Mass-producible and efficient optical antennas with CMOS-fabricated nanometer-scale gap. *Opt. Express* **2013**, *21*, 16561−16569.

(13) Dhakal, A.; Subramanian, A. Z.; Wuytens, P.; Peyskens, F.; Le Thomas, N.; Baets, R. Evanescent excitation and collection of spontaneous Raman spectra using silicon nitride nanophotonic waveguides. *Opt. Lett.* **2014**, *39*, 4025−4028.

(14) Peyskens, F.; Subramanian, A. Z.; Neutens, P.; Dhakal, A.; Van Dorpe, P.; Le Thomas, N.; Baets, R. Bright and dark plasmon resonances of nanoplasmonic antennas evanescently coupled with a silicon nitride waveguide. *Opt. Express* **2015**, *23*, 3088−3101.

(15) Arnaud, L.; Bruyant, A.; Renault, M.; Hadjar, Y.; Salas-Montiel, R.; Apuzzo, A.; Lérondel, G.; Morand, A.; Benech, P.; Le Coarer, E.; Blaize, S. Waveguide-coupled nanowire as an optical antenna. *J. Opt. Soc. Am. A* **2013**, *30*, 2347−2355.

(16) Arango, F. B.; Kwadrin, A.; Koenderink, A. F. Plasmonic Antennas Hybridized with Dielectric Waveguides. *ACS Nano* **2012**, *6*, 10156−10167.

(17) Février, M.; Gogol, P.; Aassime, A.; Mégy, R.; Delacour, C.; Chelnokov, A.; Apuzzo, A.; Blaize, S.; Lourtioz, J.-M.; Dagens, B. Giant Coupling Effect between Metal Nanoparticle Chain and Optical Waveguide. *Nano Lett.* **2012**, *12*, 1032−1037.

(18) Février, M.; Gogol, P.; Lourtioz, J.-M.; Dagens, B. Metallic nanoparticle chains on dielectric waveguides: coupled and uncoupled situations compared. *Opt. Express* **2013**, *21*, 24504−24513.

(19) Février, M.; Gogol, P.; Barbillon, G.; Aassime, A.; Mégy, R.; Bartenlian, B.; Lourtioz, J.-M.; Dagens, B. Integration of short gold nanoparticles chain on SOI waveguide toward compact integrated biosensors. *Opt. Express* **2012**, *20*, 17402−17410.

(20) Chamanzar, M.; Xia, Z.; Yegnanarayanan, S.; Adibi, A. Hybrid integrated plasmonic-photonic waveguides for on-chip localized surface plasmon resonance (LSPR) sensing and spectroscopy. *Opt. Express* **2013**, *21*, 32086−32098.

(21) Lin, S.; Zhu, W.; Jin, Y.; Crozier, K. B. Surface-Enhanced Raman Scattering with Ag Nanoparticles Optically Trapped by a Photonic Crystal Cavity. *Nano Lett.* **2013**, *13*, 559−563.

(22) Kong, L.; Lee, C.; Earhart, C. M.; Cordovez, B.; Chan, J. W. A nanotweezer system for evanescent wave excited surface enhanced Raman spectroscopy (SERS) of single nanoparticles. *Opt. Express* **2015**, *23*, 6793−6802.

(23) Measor, P.; Seballos, L.; Yin, D.; Zhang, J. Z.; Lunt, E. J.; Hawkins, A. R.; Schmidt, H. On-chip surface-enhanced Raman scattering detection using integrated liquid-core waveguides. *Appl. Phys. Lett.* **2007**, *90*, 211107−1−211107−3.

(24) Fan, M.; Andrade, G. F. S.; Brolo, A. G. A review on the fabrication of substrates for surface enhanced Raman spectroscopy and their applications in analytical chemistry. *Anal. Chim. Acta* **2011**, *693*, 7−25.

(25) Mahmoud, M. A. Surface-Enhanced Raman Spectroscopy of Double-Shell Hollow Nanoparticles: Electromagnetic and Chemical Enhancements. *Langmuir* **2013**, *29*, 6253−6261.

(26) Martens, D.; Subramanian, A.; Pathak, S.; Vanslembrouck, M.; Bienstman, P.; Bogaerts, W.; Baets, R. Compact silicon nitride arrayed waveguide gratings for very near-infrared wavelengths. *IEEE Photonics Technol. Lett.* **2015**, *27*, 137−140.

(27) Pelton, M. Modified spontaneous emission in nanophotonic structures. *Nat. Photonics* **2015**, *9*, 427−435.

(28) Tame, M. S.; McEnery, K. R.; Özdemir, S. K.; Lee, J.; Maier, S. A.; Kim, M. S. Quantum plasmonics. *Nat. Phys.* **2013**, *9*, 329−340.

(29) Johnson, P. B.; Christy, R. W. Optical Constants of the Noble Metals. *Phys. Rev. B* **1972**, *6*, 4370−4379.

(30) Haynes, W. M., Eds. *CRC Handbook of Chemistry and Physics*, 95th ed. (Internet Version 2015); CRC/Taylor and Francis, 2015.

(31) Thomas, M.; Mühlig, S.; Deckert-Gaudig, T.; Rockstuhl, C.; Deckert, V.; Marquetand, P. Distinguishing chemical and electromagnetic enhancement in surface-enhanced Raman spectra: The case of para-nitrothiophenol. *J. Raman Spectrosc.* **2013**, *44*, 1497−1505.

DOI: 10.1021/acsphotonics.5b00487
ACS Photonics 2016, 3, 102−108